

Controlled creation of point defects in three-dimensional colloidal crystals

Max P. M. Schelling  and Janne-Mieke Meijer 

Department of Applied Physics and Science Education, Eindhoven University of Technology,

P.O. Box 513, 5600 MB Eindhoven, The Netherlands

and Institute for Complex Molecular Systems, Eindhoven University of Technology, P.O. Box 513, 5600 MB Eindhoven, The Netherlands

 (Received 10 November 2023; revised 17 April 2024; accepted 6 May 2024; published 4 June 2024)

Crystal defects crucially influence the properties of crystalline materials and have been extensively studied. Even for the simplest type of defect—the point defect—however, basic properties such as their diffusive behavior, and their interactions, remain elusive on the atomic scale. Here, we demonstrate *in situ* control over the creation of isolated point defects in a three-dimensional (3D) colloidal crystal allowing insight on a single-particle level. Our system consists of thermoresponsive microgel particles embedded in a crystal of nonresponsive colloids. Heating this mixed-particle system triggers the shrinking of the embedded microgels, which then vacate their lattice positions, creating vacancy-interstitial pairs. We use temperature-controlled confocal laser scanning microscopy to verify and visualize the formation of the point defects. In addition, by reswelling the microgels we quantify the local lattice distortion around an interstitial defect. Our experimental model system provides a unique opportunity to shed light on the interplay between point defects, on the mechanisms of their diffusion, on their interactions, and on collective dynamics.

DOI: [10.1103/PhysRevE.109.L062601](https://doi.org/10.1103/PhysRevE.109.L062601)

Introduction. In any crystal, structural imperfections (defects) are thermodynamically bound to occur. Defects crucially influence the mechanical, structural, and optical properties of materials and for this reason have remained extensively studied [1,2]. While defects may have desirable effects—they may enhance the conductive properties of semiconductors [3], or may act as active sites in catalysis [4]—their presence can also be undesirable, causing metal fatigue or the softening of nanocrystalline metals [5]. Of particular interest are point defects (vacancies and interstitials). While these distort the lattice only locally, they play a crucial role in bulk properties such as diffusion creep and material degradation [2]. A dramatic example of this occurs in radiation-shielding materials, where high-energy particles generate vacancy-interstitial pairs (Frenkel pairs) that are known to greatly compromise material strength and integrity [6–8]. However, despite remarkable progress in high-resolution electron microscopy studies of defect dynamics [9–12], the atomic details of the local lattice distortion, diffusion, and collective organization of point defects remain elusive.

Here, we present an experimental platform offering a window into the basic properties and dynamics of point defects in crystalline materials using colloids. Colloids have played a central role as convenient experimental model systems to study many physical phenomena, such as phase transitions and the glass transition [13–19]. Colloidal particles are small enough to experience Brownian motion, causing them to exhibit equilibrium phase behavior similar to atomic and molecular systems. Importantly, though, they are large enough to be readily observed, with single-particle resolution, using optical microscopy. For example, experiments on defects in three-dimensional (3D) colloidal crystals have already provided unique insight into dislocations (line defects)—

their nucleation [20], dynamics [21], interactions [22], and width [23]. Experiments on *point* defects, however, have so far been limited to two-dimensional (2D) systems [24], for instance, employing laser optical tweezers to artificially introduce vacancies and interstitials, revealing the equilibrium configurations [25], diffusion [26,27], defect string formation [28] and kinetics [29,30]. So far, point defects in 3D colloidal crystals remain underexamined because experimental point defect concentrations are low [31] and optical tweezers cannot be used to remove or add particles in 3D crystals without distorting the full crystal [32].

In this Letter, we overcome the challenge of the controlled generation of point defects in three dimensions in an experimental responsive colloidal system that breaks ground for point defect studies in three dimensions. We demonstrate that

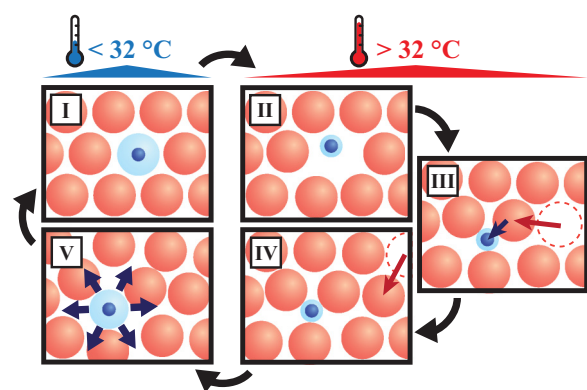


FIG. 1. By embedding size-tunable microgels in a crystal of nonresponsive colloids, the formation of a vacancy-interstitial pair is induced. Subsequently, the lattice can be strained by reswelling of interstitial microgels.

our system can induce both vacancies and interstitials, and we present the experimental determination of local lattice distortions around an interstitial in three dimensions. Our system consists of thermoresponsive poly(*N*-isopropyl acrylamide) (PNIPAM) microgels embedded in a crystal of nonresponsive latex colloids and is schematically depicted in Fig. 1. The size of PNIPAM microgels is reversibly tunable with temperature. At low temperatures the microgels are swollen with water, while above the volume phase transition temperature (VPTT, around 32 °C) the microgels collapse [33,34], resulting in a change in their volume fraction that has been extensively studied in bulk [17,35,36]. In our system, by employing a low concentration of microgels, they will take up a lattice position in a nonresponsive crystal at low temperatures. Heating the system across the VPTT leads to a significant decrease of the microgel size and allows them to migrate to an interstitial lattice site, which effectively results in the formation of a vacancy-interstitial pair. Subsequently, by lowering the temperature, reswelling of a microgel that is located on an interstitial lattice site results in a significant local strain that we can visualize on a single-particle level. We measured the resulting lattice distortion around these interstitials and found an anisotropic strain with a decay that is comparable to results from theory [2,37] and simulations [38,39].

Colloidal model system. To realize the system presented in Fig. 1, two types of colloidal particles were synthesized. The microgels consist of a fluorescent, nonresponsive core of poly(2,2,2-trifluoro ethyl methacrylate) (PTFEMA) and a cross-linked PNIPAM microgel shell [40]. Fluorescent latex particles consisting of PTFEMA and coated with a thin layer of poly(oligo-ethylene glycol methacrylate) were used as non-responsive colloids (see Supplemental Material for details about the synthesis and characterization [41]). Figure 2(a) shows the hydrodynamic diameter of the particles versus temperature as determined with dynamic light scattering (DLS). The VPTT of the microgels is determined as 32.3 °C (see Fig. S1(a) [41]). Below the VPTT (20.0 °C), both particles have a similar size $d_H \approx 1.0 \mu\text{m}$, ensuring that the microgels can replace a PTFEMA particle in the crystal. Above the VPTT, the microgels decrease significantly in size to $d_H = 0.38 \pm 0.01 \mu\text{m}$ (37.0 °C), making them small enough to occupy an octahedral site of $0.41 \mu\text{m}$ in a close-packed crystal of $1.0\text{-}\mu\text{m}$ colloids.

The mixed system consists of a small fraction of microgels (0.5%–1%) in a crystal of nonresponsive colloids with volume fraction 0.57 ± 0.04 (see Supplemental Material for details [41]). The colloids adopt a random-hexagonal close packed (*rhcp*) structure upon sedimentation, which is essentially a mixture of face-centered cubic (*fcc*) and hexagonal close packed (*hcp*) crystal structures. Figure 2(b) (upper panel) shows a 2D confocal laser scanning microscopy (CLSM) image of the mixed crystal, where the hexagonal *rhcp* planes are parallel to the flat substrate. Here, the microgels clearly take up a single lattice site, although only the fluorescent microgel cores are visible, since the shells are not fluorescently labeled. To change the microgel size in the mixed crystal, temperature-controlled CLSM experiments were performed in two and three dimensions using a VAHEAT (Interference) temperature controller [42]. Particle positions were obtained using

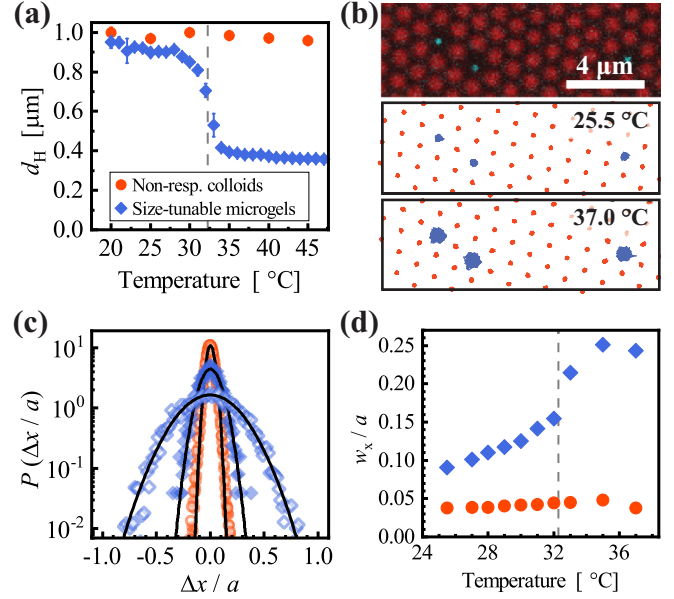


FIG. 2. (a) Hydrodynamic diameter d_H as a function of temperature for both nonresponsive PTFEMA colloids and size-tunable PNIPAM microgels. The dashed line denotes the VPTT of the microgels. Error bars represent one standard deviation. (b) CLSM image of the mixed crystal at 25.5 °C (upper panel), and 2D trajectories (30 s, 15 fps) in the same field of view at 25.5 °C (middle panel) and 37.0 °C (lower panel). (c) Self-part of the one-dimensional (1D) Van Hove function for reduced displacements $\Delta x/a$, where a is the nearest-neighbor distance ($a = 1.09 \mu\text{m}$) and lag time $\tau = 1$ s. Solid symbols are at 25.5 °C and open symbols are at 37.0 °C. Solid lines are Gaussian fits using Eq. (1). (d) Reduced width w_x/a of the 1D Van Hove functions as function of temperature. Dashed line represents the VPTT from DLS.

TRACKPY [43] based on the Crocker-Grier centroid-finding algorithm [44].

To confirm that temperature changes only influence the microgel size and do not affect the colloidal crystal structure or dynamics, we studied the mixed system behavior between 25.5 °C and 37.0 °C. Figure 2(b) shows 2D trajectories of both particles at 25.5 °C (middle panel) and 37.0 °C (lower panel). The trajectories clearly show that the microgels, due to their smaller size, are more mobile on their lattice site above the VPTT. In addition, we did not observe any change in the overall crystal lattice positions.

To quantify the particle dynamics, we calculate the self-part of the Van Hove correlation function from the particle trajectories, which gives the probability distribution $P(\Delta x, \tau)$ of particle displacements Δx along the x coordinate within a lag time τ . Figure 2(c) shows the probability distributions for $\tau = 1$ s for both particles (the width of the distributions does not increase for larger τ ; see Fig. S3 [41]). Only for the microgels the Van Hove function shows a significant broadening with increasing temperature. The width w_x of the distributions at temperatures around the VPTT was obtained by fitting

$$P(\Delta x, \tau) = \frac{1}{w_x \sqrt{2\pi}} \exp\left(-\frac{\Delta x^2}{2w_x^2}\right). \quad (1)$$

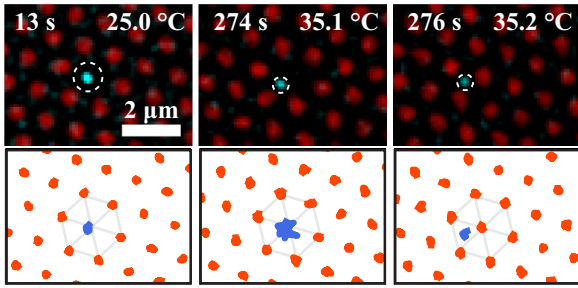


FIG. 3. Upper panels display bandpassed CLSM images showing the formation of a vacancy-interstitial pair induced by heating across the VPTT (2.4 °C/min after 20-s equilibration at 25 °C). The vacancy is formed in an adjacent layer. Dashed circles are an indication of the microgel size. Lower panels show the corresponding trajectories (1 s).

Figure 2(d) shows w_x for both the PTFEMA colloids and PNIPAM microgels at each investigated temperature. As expected, no substantial change in w_x was observed for the nonresponsive colloids. The sharp increase in w_x for the PNIPAM microgels is a result of their collapse around the VPTT. The size change of the microgels clearly still happens in a similar temperature regime in the dense colloidal crystal of PTFEMA particles as under dilute conditions [see DLS measurements in Fig. 2(a)]. These results confirm that by controlling the temperature we can finely tune the size of the embedded microgels without affecting the rest of the crystal.

Formation of vacancy-interstitial pairs. To create point defects, we increased the temperature of the mixed colloidal crystal above the VPTT slowly. Over time, the collapsed microgels are able to spontaneously move from a regular lattice site to an interstitial position, forming the expected vacancy-interstitial pair. Figure 3 shows CLSM images (upper panels) and 2D particle trajectories (lower panels) of this observed vacancy-interstitial pair formation. At the start at low temperature, the microgel is clearly embedded in the nonresponsive crystal with reduced mobility. After heating the crystal to above the VPTT, the microgel starts to rattle in its cage. Since the microgel collapse leads to a reduced local pressure (similar to the case of a true vacancy [45]), at a certain moment a colloid from an adjacent layer “hops” and takes up the original lattice site, thereby trapping the microgel in an interstitial site. We found that the formation of a vacancy-interstitial pair can happen in two ways. The first mechanism is that two spontaneous movements of the microgel and nonresponsive particle occur at the same time, as shown in Fig. 3. The second mechanism is the diffusion of the collapsed microgel to an octahedral interstitial site further away by passing between two nonresponsive colloids, leaving behind a vacancy in the originally occupied lattice site, which we observed less frequently. For both processes there is an associated energy barrier that depends on the density of the crystal and the size of the collapsed microgel relative to the other colloids. In addition, we observed that after the creation of the vacancy-interstitial pair, the pair can split up by diffusion, resulting in isolated vacancies and interstitials, which allows us to study these defects separately as well.

The vacancy-interstitial pairs induced in this colloidal system are analogous to Frenkel pairs found in atomic systems. In metals, this type of defect does generally not occur under normal conditions due to the high formation energy of interstitials, but is predominantly generated during particle irradiation. In ionic solids, Frenkel defects can be formed spontaneously because there is usually a significant size difference between the cation and anion. For the same reason, in the system presented here, only collapsed microgels are small enough to move to an interstitial site without significantly distorting the lattice.

Inducing strain with interstitial microgels. In our colloidal system we have the additional control that, once a collapsed microgel is on an interstitial site, lowering the temperature across the VPTT will result in reswelling of the microgel. This local swelling provides the opportunity to apply a stress around the interstitial site and to visualize how this distorts the local crystal structure, a process that lies at the core of interstitial interactions and agglomeration. To investigate the local strain due to reswelling of interstitial microgels, we slowly cooled a mixed system with interstitial microgels across the VPTT, while simultaneously imaging the system in three dimensions with CLSM. Figure 4(a) shows an overlay of CLSM images of an interstitial microgel and the hexagonal planes directly above and below the microgel [in a pure *fcc* crystal these are the (111) planes]. For clarity, a 3D reconstruction [46] using the tracked particle positions is given below the CLSM images. The images show that cooling across the VPTT results indeed in the swelling of the microgel and a distortion of the local lattice. We note that this distortion is relatively small and therefore difficult to observe by merely looking at the CLSM images. At a certain point, a stress relaxation event occurs that results in a jump of the (nearly) swollen microgel to a regular lattice site, pushing away the colloid that originally occupies this site. These stress relaxations happen so fast that we have not been able to fully visualize the event in three dimensions with CLSM with high temporal resolution (our fastest frame rate was 0.23 frames per second for a $256 \times 256 \times 101$ image stack). The pushed particles appear to move toward the disordered layer of colloids at the substrate, which is comparable to how in atomic systems disordered interfaces such as grain boundaries act as the defect sinks.

To determine the exact temperature range in which the buildup of lattice strain takes place, we first analyzed the Voronoi cell volume of the interstitial microgel as function of temperature [47]. Figure 4(b) shows the Voronoi cell volume and the average value during the cooling process for 14 interstitial microgels. We used cooling rates of -1.0 °C/min and -3.2 °C/min for the experiments, but we do not observe a significant difference in the results (see Fig. S4(a) [41]). The curve shows that by decreasing temperature, the microgel swells and causes an increase in the Voronoi cell volume, indicating the interstitial microgel indeed pushes its direct nearest neighbors. The Voronoi cell volume of the microgels remains constant *above* the VPTT (32.3 °C, dashed vertical line) and only increases once the temperature is *below* the VPTT. Hence, only from this temperature onward the microgels start to significantly strain the crystal. For <29 °C, a constant Voronoi cell volume is present as the microgels

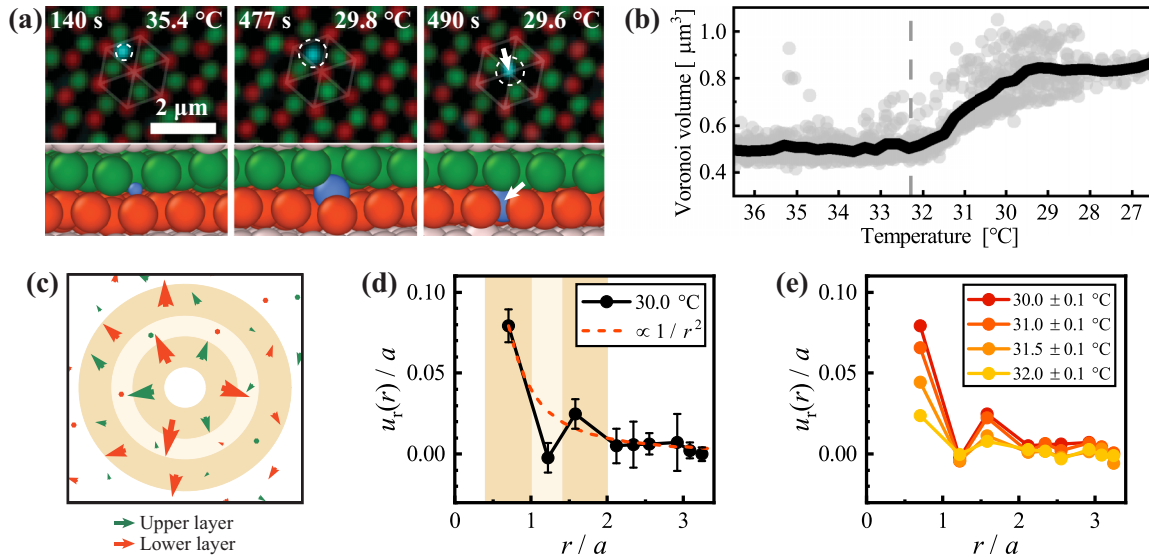


FIG. 4. (a) Upper panels show an overlay of bandpassed CLSM images of the layers above (green) and below (red) an interstitial microgel (dashed circle), while the lower panels show 3D renderings at the same points in time. Upon cooling across the VPTT, the interstitial microgels (left panels) induce a local distortion on the crystal lattice (middle panels). A relaxation event involving a nearby defect causes the (nearly) swollen microgel to take up a regular lattice site (right panels). (b) Voronoi cell volume of interstitial microgels while cooling across the VPTT (dashed line). Gray points are obtained from separate measurements of 14 microgels; the black line is a moving average. (c) Particle displacements of the layer above and below a swelling interstitial microgel at $30.0\text{ °C} \pm 0.1\text{ °C}$, measured relative to the average positions in the range $37\text{ °C} - 35\text{ °C}$. The length of the arrows are scaled by a factor 20. (d) Reduced radial component of the displacements u_r/a around an interstitial microgel as function of the distance r/a from the microgel (average of five microgels), where a is the nearest-neighbor distance ($a \approx 1.09\text{ }\mu\text{m}$). Error bars denote 95% confidence intervals obtained from the standard error. The first three layers are highlighted and correspond to the rings shown in (c). (e) Radial component of the displacements measured at different temperatures (an average of at least five microgels). Data obtained at $30.0\text{ °C} \pm 0.1\text{ °C}$ is the same as in (d). Error bars are omitted but are typically of the same magnitude as in (d).

typically have moved from an interstitial site to a regular crystal lattice site, with some exceptions that remained at the interstitial site (see Fig. S4(b) [41]).

To quantify the strain caused by the swelling of interstitial microgels, we measured the local distortion that occurs in the surrounding crystal around a single interstitial microgel between 32 °C and 30 °C . Figure 4(c) shows the typical particle displacements measured around a single microgel by comparing the average nonresponsive particle positions in the range $37\text{ °C} - 35\text{ °C}$ (i.e., fully collapsed microgel) to their positions at $30.0\text{ °C} \pm 0.1\text{ °C}$ (nearly swollen microgel on interstitial site). Similar to Fig. 4(a), the hexagonal planes above (green arrows) and below (red arrows) the interstitial microgel are shown. The arrows show that the strain is not isotropic: the displacements are strongest in the direction of the nearest neighbors of the interstitial microgel as these are pushed to accommodate the swelling microgel. Assuming a pure *fcc* structure, this displacement occurs along the cubic axes (or $\langle 100 \rangle$ directions). In the second shell of colloids around the interstitial (i.e., its next-nearest neighbors), the displacements are found to be negligible, since these colloids are not pushed by the nearest neighbors. In contrast, the particles in the third shell are pushed by the nearest neighbors and show a clear displacement. This nonuniform nature of the strain is also observed in the average radial component of the particle displacements u_r around a swelling interstitial microgel as plotted in Fig. 4(d) (see Supplemental Material for more elaboration [41]). Such anisotropic strain due to the crystal lattice has also been found with simulations

[38,39] and theory [37]. We further note that the amount of distortion around an interstitial microgel can be tuned via the temperature as shown in Fig. 4(e). The results in Fig. 4(d) indicate that the measured displacements around microgels at $30.0\text{ °C} \pm 0.1\text{ °C}$ decay within a few lattice sites. The decay in the maxima of the radial displacement appears consistent with $1/r^2$, which can be rationalized using linear elasticity theory and, although an oversimplification, approximating the crystal as an isotropic continuum [2]. Interestingly, simulations of hard-sphere systems [38] suggest an exponential decay of the displacements near a self-interstitial that ranges over more lattice sites than measured here. This discrepancy is likely due to the fact that in our results obtained at 30.0 °C , the microgels are not fully swollen and are therefore slightly smaller than the colloids in the crystal [see DLS results in Fig. 2(a)]. Moreover, it is difficult to predict the actual size of a swelling microgel on an interstitial site, as microgels have a soft and deformable character, and are able to osmotically deswell in dense systems [48]. It is clear, however, that the interstitials can induce a local strain which ranges over several lattice sites into the nonresponsive crystal.

Conclusions. In summary, we present here a colloidal model system in which the creation of point defects in 3D crystals can be controlled *in situ* and visualized on a single-particle level. In this system, PNIPAM microgels are embedded into a nonresponsive colloidal crystal where these are able to take up interstitial positions when heated above 32 °C (VPTT), resulting in the formation of vacancy-interstitial pairs that are similar to Frenkel pairs found in

atomic systems. Due to the colloidal nature and unique temperature control, the system allows us to visualize the exact moment of point defect creation and their diffusion. In addition, reswelling of the microgels by lowering the temperature across the VPTT allows us to measure the local distortion induced by interstitials, which is otherwise problematic due to their rarity. We find that the local strain displays an anisotropy that is in agreement with results from theory and simulations. The system presented in this Letter opens the possibility to gain insight into point defect phenomena, such as defect interactions, as it offers *in situ* control over the formation of

both vacancies and interstitials, while their concentration can be controlled via the mixing ratio. This insight is valuable for understanding defect dynamics in atomic crystals, such as radiation shielding materials, while it could also help to adjust and improve the rational design and controlled defect engineering of complex crystals.

Acknowledgments. We thank C. Storm and L. Filion for fruitful discussions. We acknowledge T.F. Sparidans for performing DLS measurements. J.M.M. acknowledges financial support from the Netherlands Organization for Scientific Research (NWO) (016.Veni.192.119).

-
- [1] D. Hull and D. Bacon, *Introduction to Dislocations*, 5th ed. (Elsevier, New York, 2011).
- [2] R. Phillips, *Crystals, Defects and Microstructures* (Cambridge University Press, Cambridge, 2001).
- [3] P. M. Koenraad and M. E. Flatté, Single dopants in semiconductors, *Nat. Mater.* **10**, 91 (2011).
- [4] C. Xie, D. Yan, H. Li, S. Du, W. Chen, Y. Wang, Y. Zou, R. Chen, and S. Wang, Defect chemistry in heterogeneous catalysis: Recognition, understanding, and utilization, *ACS Catal.* **10**, 11082 (2020).
- [5] J. Schiøtz, F. D. Di Tolla, and K. W. Jacobsen, Softening of nanocrystalline metals at very small grain sizes, *Nature (London)* **391**, 561 (1998).
- [6] J. Knaster, A. Moeslang, and T. Muroga, Materials research for fusion, *Nat. Phys.* **12**, 424 (2016).
- [7] X.-M. Bai, A. F. Voter, R. G. Hoagland, M. Nastasi, and B. P. Uberuaga, Efficient annealing of radiation damage near grain boundaries via interstitial emission, *Science* **327**, 1631 (2010).
- [8] C. Lu, L. Niu, N. Chen, K. Jin, T. Yang, P. Xiu, Y. Zhang, F. Gao, H. Bei, S. Shi, M.-R. He, I. M. Robertson, W. J. Weber, and L. Wang, Enhancing radiation tolerance by controlling defect mobility and migration pathways in multicomponent single-phase alloys, *Nat. Commun.* **7**, 13564 (2016).
- [9] K. Arakawa, K. Ono, M. Isshiki, K. Mimura, M. Uchikoshi, and H. Mori, Observation of the one-dimensional diffusion of nanometer-sized dislocation loops, *Science* **318**, 956 (2007).
- [10] Y. Matsukawa and S. J. Zinkle, One-dimensional fast migration of vacancy clusters in metals, *Science* **318**, 959 (2007).
- [11] S. Moll, T. Jourdan, and H. Lefaix-Jeuland, Direct observation of interstitial dislocation loop coarsening in α -iron, *Phys. Rev. Lett.* **111**, 015503 (2013).
- [12] S. Chu, P. Liu, Y. Zhang, X. Wang, S. Song, T. Zhu, Z. Zhang, X. Han, B. Sun, and M. Chen, In situ atomic-scale observation of dislocation climb and grain boundary evolution in nanostructured metal, *Nat. Commun.* **13**, 4151 (2022).
- [13] U. Gasser, E. R. Weeks, A. Schofield, P. N. Pusey, and D. A. Weitz, Real-space imaging of nucleation and growth in colloidal crystallization, *Science* **292**, 258 (2001).
- [14] T. H. Zhang and X. Y. Liu, Experimental modelling of single-particle dynamic processes in crystallization by controlled colloidal assembly, *Chem. Soc. Rev.* **43**, 2324 (2014).
- [15] A. M. Alsayed, M. F. Islam, J. Zhang, P. J. Collings, and A. G. Yodh, Premelting at defects within bulk colloidal crystals, *Science* **309**, 1207 (2005).
- [16] Y. Peng, Z. Wang, A. M. Alsayed, A. G. Yodh, and Y. Han, Melting of colloidal crystal films, *Phys. Rev. Lett.* **104**, 205703 (2010).
- [17] F. Wang, D. Zhou, and Y. Han, Melting of colloidal crystals, *Adv. Funct. Mater.* **26**, 8903 (2016).
- [18] P. Yunker, Z. Zhang, and A. G. Yodh, Observation of the disorder-induced crystal-to-glass transition, *Phys. Rev. Lett.* **104**, 015701 (2010).
- [19] E. R. Weeks, Introduction to the colloidal glass transition, *ACS Macro Lett.* **6**, 27 (2017).
- [20] P. Schall, I. Cohen, D. A. Weitz, and F. Spaepen, Visualizing dislocation nucleation by indenting colloidal crystals, *Nature (London)* **440**, 319 (2006).
- [21] P. Schall, I. Cohen, D. A. Weitz, and F. Spaepen, Visualization of dislocation dynamics in colloidal crystals, *Science* **305**, 1944 (2004).
- [22] I. Svetlizky, S. Kim, D. A. Weitz, and F. Spaepen, Dislocation interactions during plastic relaxation of epitaxial colloidal crystals, *Nat. Commun.* **14**, 5760 (2023).
- [23] J. Hilhorst and A. V. Petukhov, Variable dislocation widths in colloidal crystals of soft thermosensitive spheres, *Phys. Rev. Lett.* **107**, 095501 (2011).
- [24] X. Cao, E. Panizon, A. Vanossi, N. Manini, E. Tosatti, and C. Bechinger, Pile-up transmission and reflection of topological defects at grain boundaries in colloidal crystals, *Nat. Commun.* **11**, 3079 (2020).
- [25] A. Pertsinidis and X. S. Ling, Equilibrium configurations and energetics of point defects in two-dimensional colloidal crystals, *Phys. Rev. Lett.* **87**, 098303 (2001).
- [26] A. Pertsinidis and X. S. Ling, Diffusion of point defects in two-dimensional colloidal crystals, *Nature (London)* **413**, 147 (2001).
- [27] S.-C. Kim, L. Yu, A. Pertsinidis, and X. S. Ling, Dynamical processes of interstitial diffusion in a two-dimensional colloidal crystal, *Proc. Natl. Acad. Sci. USA* **117**, 13220 (2020).
- [28] W. Lechner, D. Polster, G. Maret, P. Keim, and C. Dellago, Self-organized defect strings in two-dimensional crystals, *Phys. Rev. E* **88**, 060402(R) (2013).
- [29] W. Lechner, D. Polster, G. Maret, C. Dellago, and P. Keim, Entropy and kinetics of point defects in two-dimensional dipolar crystals, *Phys. Rev. E* **91**, 032304 (2015).
- [30] B. van der Meer, W. Qi, R. G. Fokkink, J. Van Der Gucht, M. Dijkstra, and J. Sprakel, Highly cooperative stress relaxation in two-dimensional soft colloidal crystals, *Proc. Natl. Acad. Sci. USA* **111**, 15356 (2014).

- [31] S. Pronk and D. Frenkel, Point defects in hard-sphere crystals, *J. Phys. Chem. B* **105**, 6722 (2001).
- [32] Y. Liu, K. V. Edmond, A. Curran, C. Bryant, B. Peng, D. G. A. L. Aarts, S. Sacanna, and R. P. A. Dullens, Core-shell particles for simultaneous 3D imaging and optical tweezing in dense colloidal materials, *Adv. Mater.* **28**, 8001 (2016).
- [33] R. H. Pelton and P. Chibante, Preparation of aqueous latices with *N*-isopropylacrylamide, *Colloids Surf.* **20**, 247 (1986).
- [34] Y. H. Bae, T. Okano, and S. W. Kim, Temperature dependence of swelling of crosslinked poly (N,Nalkyl substituted acrylamides) in water, *J. Polym. Sci. Part B: Polym. Phys.* **28**, 923 (1990).
- [35] M. Karg, A. Pich, T. Hellweg, T. Hoare, L. A. Lyon, J. J. Crassous, D. Suzuki, R. A. Gumerov, S. Schneider, I. I. Potemkin, and W. Richtering, Nanogels and microgels: From model colloids to applications, recent developments, and future trends, *Langmuir* **35**, 6231 (2019).
- [36] P. J. Yunker, K. Chen, M. D. Gratale, M. A. Lohr, T. Still, and A. G. Yodh, Physics in ordered and disordered colloidal matter composed of poly(N-isopropylacrylamide) microgel particles, *Rep. Prog. Phys.* **77**, 056601 (2014).
- [37] G. L. Hall, Distortion around point imperfections in simple crystals, *J. Phys. Chem. Solids* **3**, 210 (1957).
- [38] B. van der Meer, M. Dijkstra, and L. Filion, Diffusion and interactions of point defects in hard-sphere crystals, *J. Chem. Phys.* **146**, 244905 (2017).
- [39] R. M. Alkemade, M. de Jager, B. van der Meer, F. Smalenburg, and L. Filion, Point defects in crystals of charged colloids, *J. Chem. Phys.* **154**, 164905 (2021).
- [40] J. Appel, N. De Lange, H. M. Van Der Kooij, T. Van De Laar, J. B. Ten Hove, T. E. Kodger, and J. Sprakel, Temperature controlled sequential gelation in composite microgel suspensions, *Part. Part. Syst. Charact.* **32**, 764 (2015).
- [41] See Supplemental Material at <http://link.aps.org/supplemental/10.1103/PhysRevE.109.L062601> for a description of the particle synthesis and characterization, details about the CLSM experiments, and additional figures, which includes Refs. [40,49–51].
- [42] J. Icha, D. Böning, and P. Türschmann, Precise and dynamic temperature control in high-resolution microscopy with VA-HEAT, *Microscopy Today* **30**, 34 (2022).
- [43] D. B. Allan, T. Caswell, N. C. Keim, C. M. van der Wel, and R. W. Verweij, soft-matter/trackpy: Trackpy v0.5.0 (v0.5.0), Zenodo (2021), <https://github.com/soft-matter/trackpy>.
- [44] J. C. Crocker and D. G. Grier, Methods of digital video microscopy for colloidal studies, *J. Colloid Interface Sci.* **179**, 298 (1996).
- [45] N. Y. Lin, M. Bierbaum, P. Schall, J. P. Sethna, and I. Cohen, Measuring nonlinear stresses generated by defects in 3D colloidal crystals, *Nat. Mater.* **15**, 1172 (2016).
- [46] A. Stukowski, Visualization and analysis of atomistic simulation data with OVITO the Open Visualization Tool, *Modell. Simul. Mater. Sci. Eng.* **18**, 015012 (2010).
- [47] V. Ramasubramani, B. D. Dice, E. S. Harper, M. P. Spellings, J. A. Anderson, and S. C. Glotzer, FREUD: A software suite for high throughput analysis of particle simulation data, *Comput. Phys. Commun.* **254**, 107275 (2020).
- [48] A. Scotti, U. Gasser, E. S. Herman, M. Pelaez-Fernandez, J. Han, A. Menzel, L. A. Lyon, and A. Fernández-Nieves, The role of ions in the self-healing behavior of soft particle suspensions, *Proc. Nat. Acad. Sci. USA* **113**, 5576 (2016).
- [49] T. E. Kodger, R. E. Guerra, and J. Sprakel, Precise colloids with tunable interactions for confocal microscopy, *Sci. Rep.* **5**, 14635 (2015).
- [50] B. J. Frisken, Revisiting the method of cumulants for the analysis of dynamic light-scattering data, *Appl. Opt.* **40**, 4087 (2001).
- [51] T. H. Besseling, J. Jose, and A. V. Blaaderen, Methods to calibrate and scale axial distances in confocal microscopy as a function of refractive index, *J. Microsc.* **257**, 142 (2015).